Full-Wave Analysis of Dielectric Waveguides Using Tangential Vector Finite Elements

Jin-Fa Lee, *Member, IEEE*, Din-Kow Sun, *Member, IEEE*, and Zoltan J. Cendes, *Member, IEEE*

***Abstract*—A new method is presented for the analysis of dielectric waveguides. This method provides four major new contributions: 1) a transformation of variables is introduced that allows propagation constants to be computed directly; 2) $\mathscr{H}_1$(curl) tangential vector finite elements are applied to dielectric waveguides to obtain reliable approximate electromagnetic fields; 3) the Lanczos algorithm is modified to solve the required generalized eigenmatrix equation efficiently; and 4) the reaction principle is used to provide *a posteriori* error estimates for use in adaptive mesh refinement. The method described here produces reliable solutions and applies to structures that contain both electric and magnetic inhomogeneities. The answers are refined adaptively to generate waveguide eigenmodes to specified accuracy. Numerical results of an image guide, a microstrip transmission line, and a pedestal-supported stripline are shown. Computed solutions agree very well with the previously published results.**

I. Introduction

At microwave, millimeter-wave, and optical frequencies, various applications of dielectric waveguides have been suggested. In the design of these structures, it is important to calculate the propagation characteristics of the guided modes in the waveguide. According to Maxwell's equations, all of the propagating modes within an inhomogeneous structure are hybrid. Therefore, to analyze such waveguides, it is necessary to perform full-wave analysis.

Various types of analysis methods have been proposed and used. Typical methods are the method of moment [1], spectral-domain methods [2], finite difference methods [3], [4], and finite element methods [5]–[7]. The finite element method is probably the waveguide analysis method that is the most generally applicable and most versatile. With this method, it is possible to fit any polygonal shape by choosing triangular element shapes and sizes and to increase the accuracy of the solution by using high-order polynomial approximation functions.

The most serious difficulty in using the finite element method for the analysis of the modes of dielectric waveguides is the appearance of spurious modes [7], [8]. Recent reports [7]–[9] have suggested various ways to solve this problem. Rahman and Davies [7] have used a penalty function to enforce the divergence-free condition. This requires the user to select a suitable penalty function parameter. Kobelansky and Webb [8] proposed using the fields which are exactly divergence-free to be the basis functions in the finite element analysis. Such fields are themselves computed by the finite element method. This approach requires intensive computations since at least tens of basis functions need to be calculated from an auxiliary eigenmatrix equation.

In [9], Wong and Cendes observed that the occurrence of the spurious modes is due to the improper modeling of the null space of the curl operator. Subsequently, they suggested three approaches to eliminate spurious modes: using C^1 finite elements, using a consistent C^1 mesh, and using tangential elements [12]. C^1 finite elements and the C^1 consistent mesh allow the derivatives of the finite element basis functions to be continuous. In this way, the null space of the curl operator is modeled exactly and the spurious modes degenerate to eigensolutions with eigenvalue zero.

Except for the tangential element method, the above methods are all based upon a nodal finite element approach. Consequently, the resultant field is continuous in both normal and tangential components across element boundaries. For structures that have both electric and magnetic inhomogeneities, special care is required on element boundaries to ensure correct interfacial boundary conditions.

A different approach to eliminating spurious modes is to use tangential vector finite elements [9], [11], [12]. With tangential vector finite elements, only the tangential continuity of the vector field is imposed across element boundaries. The advantages of this approach are that 1) it imposes only the continuity of the tangential components of the electric and magnetic fields, as is required physically; 2) the interfacial boundary conditions are automatically obtained through the natural boundary conditions

Manuscript received March 12, 1990; revised December 10, 1990.

J.-F. Lee was with the Ansoft Corporation, Pittsburgh, PA. He is now with the Department of Electrical and Computer Engineering, University of Illinois, Urbana, IL 61801.

D.-K. Sun is with the Ansoft Corporation, Commerce Court Building 660, Pittsburgh, PA 15219.

Z. J. Cendes is with the Ansoft Corporation, Commerce Court Building 660, Pittsburgh, PA 15219, and with the Department of Electrical and Computer Engineering, Carnegie Mellon University, Pittsburgh, PA 15213.

IEEE Log Number 9101015.

0018-9480/91/0800-1262$01.00 ©1991 IEEE

built into the variational principle [12]; and 3) Dirichlet boundary condition can be easily set along the element edges. Various families of tangential elements are discussed in [11]. The lowest order tangential vector finite elements are edge elements [10] in which the unknown variables are associated with the edges of the element.

In this paper, we present the application of the high-order $\mathscr{H}_1$(curl) tangential vector finite elements to model dielectric waveguides. The formulation employs a variable transformation that allows the propagation constants in waveguides to be computed at a specified frequency rather than the other way around. In addition, an *a posteriori* error criterion based on the reaction concept is used to refine the finite element mesh adaptively.

II. Numerical Procedure

In the full-wave analysis of dielectric waveguides, it is necessary to solve the following boundary value problem (BVP):

$$\begin{aligned} \nabla \times \frac{1}{\mu_r} \nabla \times \mathscr{E} - k^2 \epsilon_r \mathscr{E} &= 0 \qquad \text{in } \Omega \\ \mathscr{E} \times n &= 0 \qquad \text{on } \Gamma_1 \\ \nabla \times \mathscr{E} \times n &= 0 \qquad \text{on } \Gamma_2 \end{aligned} \tag{1}$$

where Ω is the cross section of the guiding structure whose boundary is divided into two parts: the electric wall Γ_1 and the magnetic wall Γ_2. Here, the electric field is assumed to have a z dependence as $\mathscr{E} = \boldsymbol{E}(x, y)\exp(-j\beta z)$, where β is the propagation constant.

The corresponding variational functional for the BVP (1) can be written as [13]

$$\begin{aligned} \mathscr{F}(\mathscr{E}) &= \int_\Omega \frac{1}{\mu_r} |\nabla \times \mathscr{E}|^2 - k^2 \epsilon_r |\mathscr{E}|^2 \, d\Omega \\ &= \int_\Omega \frac{1}{\mu_r} \left[|\nabla_\tau \mathscr{E}_z + j\beta \mathscr{E}_\tau|^2 + |\nabla_\tau \times \mathscr{E}_\tau|^2 \right] \\ &\qquad - k^2 \epsilon_r |\mathscr{E}|^2 \, d\Omega \end{aligned} \tag{2}$$

where $\mathscr{E}_\tau = \mathscr{E}_x \boldsymbol{a}_x + \mathscr{E}_y \boldsymbol{a}_y$ and $\nabla_\tau = \partial_x \boldsymbol{a}_x + \partial_y \boldsymbol{a}_y$.

There are two approaches in solving eigenproblem (1) by using the functional in (2). One is to solve for k^2 with the propagation constant β given. The other is to specify the operating frequency and solve for the propagation constant β. As pointed out in [14], the latter is preferred in practical device design. Therefore, in this paper, we present a numerical methodology to analyze dielectric waveguides using the second approach.

A. Transformation of Variables

Imposing the operating frequency in functional (2) results in a quadratic eigenmatrix equation for β that is very difficult and expensive to solve. Furthermore, β is real for a propagating mode and imaginary for an evanescent mode. Thus, this approach requires the solution of complex eigenvalues. However, these two problems can be eliminated by introducing the following transformation of variables:

$$\begin{aligned} e_x &= \beta \mathscr{E}_x \\ e_y &= \beta \mathscr{E}_y \\ e_z &= -j \mathscr{E}_z. \end{aligned} \tag{3}$$

With the variable transformation (3), the functional (2) can be rewritten as

$$\begin{aligned} \mathscr{F}(\boldsymbol{e}) = \int_\Omega \beta^2 \left[\frac{1}{\mu_r} |\nabla_\tau e_z + \boldsymbol{e}_\tau|^2 - k^2 \epsilon_r |e_z|^2 \right] - k^2 \epsilon_r |\boldsymbol{e}_\tau|^2 \\ + \frac{1}{\mu_r} |\nabla_\tau \times \boldsymbol{e}_\tau|^2 \, d\Omega. \end{aligned} \tag{4}$$

In the functional (4), only k^2 and β^2 are involved. Thus, extremizing the functional (4) with k^2 as the given parameter, we have an eigenmatrix equation to solve for the eigenvalues β^2. Furthermore, the eigenvalues will be real since β^2 is positive for a propagating mode and negative for an evanescent mode.

The Euler equation that corresponds to the functional (4) is

$$\nabla_\tau \times \frac{1}{\mu_r} \nabla_\tau \times \boldsymbol{e}_\tau - \frac{\beta^2}{\mu_r} \nabla_\tau e_z + \frac{\beta^2}{\mu_r} \boldsymbol{e}_\tau = k^2 \epsilon_r \boldsymbol{e}_\tau \tag{5a}$$

$$\beta^2 \left(\nabla_\tau \cdot \frac{1}{\mu_r} \nabla_\tau e_z - \nabla_\tau \cdot \frac{1}{\mu_r} \boldsymbol{e}_\tau \right) = \beta^2 k^2 \epsilon_r e_z \tag{5b}$$

and the boundary conditions are

$$\begin{aligned} \hat{n} \times \boldsymbol{e} &= 0 \qquad \text{on } \Gamma_1 \\ \left.\begin{aligned} (\nabla_\tau e_z + \boldsymbol{e}_\tau) \cdot \hat{n} &= 0 \\ \nabla_\tau \times \boldsymbol{e}_\tau \cdot \boldsymbol{a}_z &= 0 \end{aligned}\right\} \qquad & \text{on } \Gamma_2. \end{aligned} \tag{6}$$

Applying the transverse divergence operator, $\nabla_\tau \cdot$, on both sides of (5a) results in

$$-\beta^2 \nabla_\tau \cdot \frac{1}{\mu_r} \nabla_\tau e_z + \beta^2 \nabla_\tau \cdot \frac{1}{\mu_r} \boldsymbol{e}_\tau = k^2 \nabla_\tau \cdot \epsilon_r \boldsymbol{e}_\tau. \tag{7}$$

Adding (7) to (5b) for $k^2 \neq 0$ yields

$$\nabla_\tau \cdot \epsilon_r \boldsymbol{e}_\tau + \beta^2 \epsilon_r e_z = 0. \tag{8}$$

This is Gauss's law for the source-free region. From (8), it is clear that as long as the operating frequency is not 0, solutions of (5) must satisfy the divergence-free condition.

The functional form given in (4) is symmetric. From the resulting Euler equation (5), there is a set of eigensolutions corresponding to $\beta^2 = 0$. However, the solutions of this set are not physical modes of the dielectric waveguide since e_z is arbitrary when $\beta^2 = 0$ in (5).

B. Tangential Vector Finite Elements

As mentioned earlier, several approaches can be used to eliminate spurious modes. Tangential vector finite elements are preferred because they most closely match the mathematical and physical requirements of modeling dielectric waveguides. In this subsection, we present the construction of the two-dimensional $\mathscr{H}_1$(curl) tangential

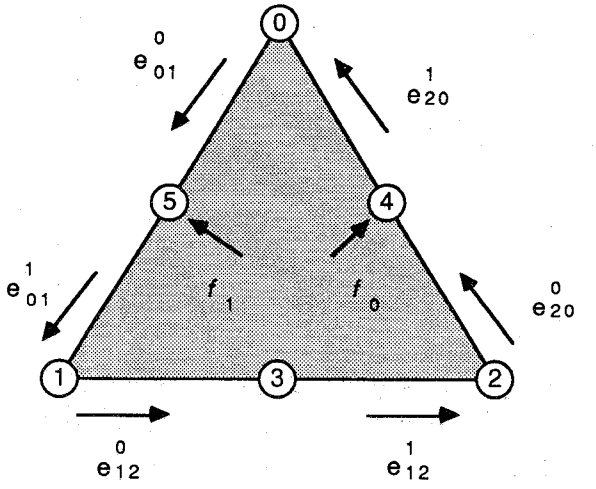

Fig. 1. The two-dimensional $\mathscr{H}_1$(curl) tangential vector finite element.

vector finite element. The two-dimensional $\mathscr{H}_1$(curl) tangential vector finite element is described mathematically as

$$\mathscr{H}_1(\text{curl}) = \left\{ \boldsymbol{e}_\tau | \boldsymbol{e}_\tau \in [L_2(\Omega)]^2, \nabla_\tau \times \boldsymbol{e}_\tau \cdot \boldsymbol{a}_z \in \mathscr{P}_1(\Omega) \right\} \tag{9}$$

where $L_2(\Omega)$ is the set of square integrable functions, and $\mathscr{P}_1(\Omega)$ is the set of piecewise-linear functions in the problem domain Ω. Since the $\mathscr{H}_1$(curl) tangential vector finite element provides a higher order approximation than is obtained from edge elements [10], it will provide more accurate numerical solutions and faster convergence in applications.

Unknowns in the $\mathscr{H}_1$(curl) element are assigned as shown in Fig. 1. The tangential projection of the field $\boldsymbol{e}_\tau$ along any edge $\{i, j\}$ is determined by two unknowns, e^0_{ij} and e^1_{ij}. In addition, two facial unknowns, f_0 and f_1, are added to provide a quadratic approximation of the normal component of the field along any two of the three edges. Notice that in Fig. 1, the edge variables e^0_{ij} and e^1_{ij} provide common unknowns across element boundaries. Thus, the tangential continuity of the field $\boldsymbol{e}_\tau$ across the element boundaries is ensured. However, the facial variables f_0 and f_1 are local unknowns associated with each separate triangular element. These two facial variables are included to provide a complete linear approximation for $\nabla_\tau \times \boldsymbol{e}_\tau$.

We can express the transverse field $\boldsymbol{e}_\tau$ by the nodal vectors $\boldsymbol{e}^i$ as

$$\boldsymbol{e}_\tau = \sum_{i=0}^{5} \boldsymbol{e}^i \alpha_i(\zeta) \tag{10}$$

where $\zeta = (\zeta_0, \zeta_1, \zeta_2)$ is the two-dimensional barycentric coordinate [15], and $\alpha_i(\zeta)$ is the second-order Lagrange interpolation polynomial at node i. However, with tangential elements the nodal vectors $\boldsymbol{e}^i$ are not independent unknowns. The edge variables e^0_{ij} and e^1_{ij} and the facial variables f_0 and f_1 are used as independent unknowns in the $\mathscr{H}_1$(curl) tangential finite element formulation.

We need to determine the nodal vectors $\boldsymbol{e}^i$ in terms of the new set of variables. At node 0, the nodal vector $\boldsymbol{e}^0$ satisfies

$$\begin{aligned} \boldsymbol{e}^0 \cdot \hat{t}_{01} &= e^0_{01} \\ \boldsymbol{e}^0 \cdot \hat{t}_{20} &= e^1_{20} \end{aligned} \tag{11}$$

where $\hat{t}_{ij}$ is the unit vector pointing from node i to node j. The solution of (11) is

$$\boldsymbol{e}^0 = \frac{e^0_{01}}{\hat{n}_{20} \cdot \hat{t}_{01}} \hat{n}_{20} + \frac{e^1_{20}}{\hat{n}_{01} \cdot \hat{t}_{20}} \hat{n}_{01} \tag{12}$$

where $\hat{n}_{ij}$ is the outward-directed normal of the edge $\{i, j\}$. By observing that $\hat{n}_{ij} \cdot \hat{t}_{jk} = -\sin\theta_j$ and $\hat{n}_{ij} \cdot \hat{t}_{ki} = \sin\theta_i$, (12) can be simplified further as

$$\boldsymbol{e}^0 = \frac{1}{\sin\theta_0} \left[e^1_{20} \hat{n}_{01} - e^0_{01} \hat{n}_{20} \right]. \tag{13}$$

Similar expressions are obtained for the nodal vectors $\boldsymbol{e}^1$ and $\boldsymbol{e}^2$. The results are

$$\begin{aligned} \boldsymbol{e}^1 &= \frac{1}{\sin\theta_1} \left[e^1_{01} \hat{n}_{12} - e^0_{12} \hat{n}_{01} \right] \\ \boldsymbol{e}^2 &= \frac{1}{\sin\theta_2} \left[e^1_{12} \hat{n}_{20} - e^0_{20} \hat{n}_{12} \right]. \end{aligned} \tag{14}$$

There are several ways to assign the facial variables f_0 and f_1. One is to define them as the quadratic part of the normal components along two of the three edges:

$$\begin{aligned} f_0 &= \left(\boldsymbol{e}^4 - \frac{\boldsymbol{e}^0 + \boldsymbol{e}^2}{2} \right) \cdot \hat{n}_{20} \\ f_1 &= \left(\boldsymbol{e}^5 - \frac{\boldsymbol{e}^0 + \boldsymbol{e}^1}{2} \right) \cdot \hat{n}_{01}. \end{aligned} \tag{15}$$

The tangential component along each edge is approximated to linear order. Thus, the nodal vectors $\boldsymbol{e}^4$ and $\boldsymbol{e}^5$ are given by

$$\begin{aligned} \boldsymbol{e}^4 &= \frac{\boldsymbol{e}^0 + \boldsymbol{e}^2}{2} + f_0 \hat{n}_{20} \\ \boldsymbol{e}^5 &= \frac{\boldsymbol{e}^0 + \boldsymbol{e}^1}{2} + f_1 \hat{n}_{01} \end{aligned} \tag{16}$$

The vector $\boldsymbol{e}^3$ is simply the linear average of $\boldsymbol{e}^1$ and $\boldsymbol{e}^2$:

$$\boldsymbol{e}^3 = \frac{\boldsymbol{e}^1 + \boldsymbol{e}^2}{2}. \tag{17}$$

Substituting (13), (14), (16), and (17) into (10), the transverse field $\boldsymbol{e}_\tau$ within the triangular element is given as

$$\begin{aligned} \boldsymbol{e}_\tau = \sum_{i=0}^{2} \frac{\zeta_i}{\sin\theta_i} \left[e^1_{ki} \hat{n}_{ij} - e^0_{ij} \hat{n}_{ki} \right] \\ + f_0 \hat{n}_{20} (4\zeta_0\zeta_2) + f_1 \hat{n}_{01} (4\zeta_0\zeta_1) \end{aligned} \tag{18}$$

where the indices i, j, and k are cyclic modulo 3. From

expression (18), we can write $\nabla_\tau \times e_\tau$ as

$$\nabla_\tau \times e_\tau = \frac{1}{\sin\theta_t}\left[e^1_{kl}\nabla_\tau\zeta_l \times \hat{n}_{ij} - e^0_{ij}\nabla_\tau\zeta_i \times \hat{n}_{kl}\right] + f_0[4\zeta_0\nabla_\tau\zeta_2 + 4\zeta_2\nabla_\tau\zeta_0]\times\hat{n}_{20} + f_1[4\zeta_0\nabla_\tau\zeta_1 + 4\zeta_1\nabla_\tau\zeta_0]\times\hat{n}_{01}. \quad (19)$$

This can be reduced further to

$$\nabla_\tau \times e_\tau = \sum_{i=0}^{2}\frac{l_{jk}}{2A}\left[e^1_{kl} + e^0_{ij}\right]a_z + \frac{2}{A}f_0[l_{01}\sin\theta_0\zeta_0 - l_{12}\sin\theta_2\zeta_2]a_z + \frac{2}{A}f_1[l_{12}\sin\theta_1\zeta_1 - l_{20}\sin\theta_0\zeta_0]a_z \quad (20)$$

where A is the area of the triangle, and l_{ij} is the length of edge $\{i,j\}$. Equation (20) is obtained with the aid of the following equations:

$$\nabla_\tau\zeta_i = -\frac{l_{jk}}{2A}\hat{n}_{jk}$$
$$\hat{n}_{ij}\times\hat{n}_{jk} = \sin\theta_j a_z$$
$$\hat{n}_{ij}\times\hat{n}_{ki} = -\sin\theta_i a_z. \quad (21)$$

It is apparent from (20) that the two facial variables f_0 and f_1 provide the required linear terms in $\nabla_\tau \times e_\tau$, while the edge variables together contribute the constant term. Therefore, expression (18) describes the desired two-dimensional $\mathscr{H}_1$(curl) tangential vector finite element.

Since a_z is always normal to the waveguide cross section and tangential to material interfaces, it is natural to use Lagrange interpolation polynomials to model the e_z component. However, to be consistent with the $\mathscr{H}_1$(curl) element, the approximation for e_z must be complete to second order. The reason is as follows: the curl of the field e can be written as $\nabla\times e = (\nabla_\tau e_z + e_\tau)\times a_z + \nabla_\tau \times e_\tau$. Since $\nabla_\tau \times e_\tau$ is complete to the first order, the gradient field $\nabla_\tau e_z$ should also be complete to first order. Therefore, we need to use second-order approximation polynomials to model e_z.

C. Modified Lanczos Algorithm

1) The Eigenmatrix Equation: As described in the previous subsection, the vector function space $\mathscr{M}$ for the trial field e is

$$\mathscr{M} = \left\{\begin{bmatrix} e_\tau \\ e_z\end{bmatrix}\middle| e_\tau \in \mathscr{H}_1(\text{curl}), e_z \in \mathscr{P}_2(\Omega)\right\}. \quad (22)$$

Applying (22) to the functional (4) and carrying out the integration gives

$$\mathscr{F}(e) = [e^*_\tau e^*_z]\begin{bmatrix}\mathscr{A} & 0\\ 0 & 0\end{bmatrix}\begin{bmatrix}e_\tau\\ e_z\end{bmatrix} + \beta^2[e^*_\tau e^*_z]\begin{bmatrix}\mathscr{B} & \mathscr{C}^t\\ \mathscr{C} & \mathscr{D}\end{bmatrix}\begin{bmatrix}e_\tau\\ e_z\end{bmatrix} \quad (23)$$

where

$$e^*_\tau\mathscr{A}e_\tau = \int_\Omega \frac{1}{\mu_r}|\nabla_\tau\times e_\tau|^2 - k^2\epsilon_r|e_\tau|^2\,d\Omega$$
$$e^*_\tau\mathscr{B}e_\tau = \int_\Omega \frac{1}{\mu_r}|e_\tau|^2\,d\Omega$$
$$e^*_\tau\mathscr{C}e_z = \frac{1}{2}\int_\Omega \frac{1}{\mu_r}e^*_\tau\cdot\nabla_\tau e_z\,d\Omega$$
$$e^*_z\mathscr{D}e_z = \int_\Omega \frac{1}{\mu_r}|\nabla_\tau e_z|^2 - k^2\epsilon_r|e_z|^2\,d\Omega. \quad (24)$$

The stationary point of the functional (23) is also the solution of the following generalized eigenmatrix equation:

$$\begin{bmatrix}\mathscr{A} & 0\\ 0 & 0\end{bmatrix}\begin{bmatrix}e_\tau\\ e_z\end{bmatrix} = -\beta^2\begin{bmatrix}\mathscr{B} & \mathscr{C}^t\\ \mathscr{C} & \mathscr{D}\end{bmatrix}\begin{bmatrix}e_\tau\\ e_z\end{bmatrix}. \quad (25)$$

Notice that the matrix on the left side of (25) is singular. Therefore, there are degenerate eigenvectors that correspond to $\beta^2 = 0$. With $\beta^2 = 0$, these eigenvectors do not satisfy $\mathscr{C}e_\tau + \mathscr{D}e_z = 0$. Thus, they are nonphysical solutions introduced by the variable transformation (3).

From the generalized eigenmatrix equation (25), it is apparent that the nonphysical solutions that correspond to $\beta^2 = 0$ form a vector function space Λ, where

$$\Lambda = \left\{\begin{bmatrix}e_\tau\\ e_z\end{bmatrix}\middle| e_\tau \equiv 0,\ e_z \neq 0\right\}. \quad (26)$$

The suppression of these nonphysical solutions in the Lanczos algorithm [16] is the subject of the next subsection.

Assuming the waveguide is lossless, it can be verified that there exists an upper bound $\Theta^2 = k^2\mu_{\max}\epsilon_{\max}$ for the eigenvalue β^2, where $\mu_{\max}$ is the maximum relative permeability and $\epsilon_{\max}$ is the maximum relative permittivity of the materials within the waveguide. Physically, Θ is the propagation constant of a TEM wave in a homogeneous medium with material properties $\mu_{\max}$ and $\epsilon_{\max}$.

By using the upper bound Θ^2, we can rewrite (25) as

$$\begin{bmatrix}\mathscr{B} & \mathscr{C}^t\\ \mathscr{C} & \mathscr{D}\end{bmatrix}\begin{bmatrix}e_\tau\\ e_z\end{bmatrix} = \frac{\Theta^2}{\Theta^2-\beta^2}\begin{bmatrix}\mathscr{B}+\frac{\mathscr{A}}{\Theta^2} & \mathscr{C}^t\\ \mathscr{C} & \mathscr{D}\end{bmatrix}\begin{bmatrix}e_\tau\\ e_z\end{bmatrix}. \quad (27)$$

The reason for transforming (25) into (27) is as follows: in a dielectric waveguide, a more dominant mode corresponds to a more positive value of β^2 and therefore $\Theta^2/(\Theta^2-\beta^2)$ will be larger. Although, in the literature [16], it is said that the Lanczos algorithm can compute either the largest or the smallest eigenvalue of the eigenmatrix equation efficiently, numerical experience indicates that the largest eigenvalue almost always converges faster than the smallest one. Thus, if we solve (27) by using the Lanczos algorithm, the eigenpairs will converge more or less by the order of dominance. In most applications where only a few eigenmodes are sought, this feature is very desirable.

2) Suppression of the Degenerate Solutions: The elements in the function space Λ are degenerate eigensolutions of (25) with $\beta^2 = 0$. The occurrence of these additional solutions in the iterative process will slow down the convergence of the desired eigenpairs in the Lanczos algorithm.

To simplify the discussion, (27) is rewritten in the following form:

$$\mathscr{P}\phi = \lambda \mathscr{Q}\phi \tag{28}$$

where

$$\mathscr{P} = \begin{bmatrix} \mathscr{B} & \mathscr{C}^t \\ \mathscr{C} & \mathscr{D} \end{bmatrix} \qquad \mathscr{Q} = \begin{bmatrix} \mathscr{B} + \dfrac{\mathscr{A}}{\Theta^2} & \mathscr{C}^t \\ \mathscr{C} & \mathscr{D} \end{bmatrix}$$

$$\lambda = \frac{\Theta^2}{\Theta^2 - \beta^2} \qquad \phi = \begin{bmatrix} e_\tau \\ e_z \end{bmatrix}. \tag{29}$$

Based on (28), the Lanczos algorithm can be described as follows: For a Krylov subspace $\mathscr{K}_m$ that is spanned by the following vectors: $\phi_0, (\mathscr{Q}^{-1}\mathscr{P})\phi_0, \cdots, (\mathscr{Q}^{-1}\mathscr{P})^{m-1}\phi_0$, where ϕ_0 is the initial guess, the Lanczos algorithm seeks to approximate each eigenpair by the pair λ^m, ϕ^m satisfying

$$\phi^m \in \mathscr{K}_m$$
$$(\mathscr{P} - \lambda^m \mathscr{Q})\phi^m \perp \mathscr{K}_m. \tag{30}$$

Since the matrices $\mathscr{P}$ and $\mathscr{Q}$ are real and symmetric, the following two properties can be proved [11]:

- Assume that (λ_1, ϕ_1) and (λ_2, ϕ_2) with $\lambda_1 \neq \lambda_2$ are two eigenpairs of (28). Then $\phi_1^t \mathscr{Q} \phi_2 = 0$.
- If the initial guess ϕ_0 satisfies $\phi_n^t \mathscr{Q} \phi_0 = 0$, $\forall \phi_n \in \Lambda$, then for any vector $\psi \in \mathscr{K}_m$ we have $\phi_n^t \mathscr{Q} \psi = 0$, $\forall \phi_n \in \Lambda$.

Thus, if we can select an initial guess ϕ_0 such that $\mathscr{Q}\phi_0 \perp \Lambda$, then additional solutions will not occur during the iterative process. This can be done, for example, by solving ϕ_0 from the following equation:

$$\mathscr{Q}\phi_0 = \begin{bmatrix} y_\tau \\ y_z \end{bmatrix} \tag{31}$$

where

$$y_\tau = \begin{bmatrix} 1 \\ 1 \\ \vdots \\ 1 \end{bmatrix} \quad \text{and} \quad y_z = \begin{bmatrix} 0 \\ 0 \\ \vdots \\ 0 \end{bmatrix}. \tag{32}$$

3) Modified Lanczos Algorithm: The Lanczos algorithm has been successfully applied to large sparse symmetric generalized eigenmatrix equations [16], [17]. Interested readers are referred to [16] and [17] for details. In equation (28), neither $\mathscr{P}$ nor $\mathscr{Q}$ is a positive definite matrix. Thus, (28) does not have the right form and we need to modify the Lanczos algorithm to it. As a result of this modification, the reduced eigenmatrix equation is not a symmetric tridiagonal matrix. It becomes a nonsymmetric, but still tridiagonal, matrix. This reduced eigenmatrix equation can be solved by calling suitable procedures from EISPACK [18]. The modified version of the Lanczos algorithm for the present application is outlined as follows:

1) Input the number of desired modes.
2) Choose a vector q such that $q \perp \Lambda$. For the Λ in (26), we choose q as

$$q = \begin{bmatrix} q_\tau \\ q_z \end{bmatrix} \tag{33}$$

where

$$q_\tau [1, 1, \cdots, 1]^t, q_z = 0. \tag{34}$$

3) Orthogonalize q against the previous converged eigenvectors ϕ_i by

$$\bar{q} = q - \sum_{i=1}^{n_c} \alpha_i \phi_i$$
$$\alpha_i = \phi_i^t \cdot q \tag{35}$$

where n_c is the number of converged eigenpairs.
4) Solve the matrix equation $\mathscr{Q}\phi = \bar{q}$ for ϕ.
5) Normalize ϕ and assign the resultant vector as v_1,

$$v_1 = \frac{\phi}{\|\phi\|}, \qquad m = 1. \tag{36}$$

6) Assign a vector f as follows:

$$f = \mathscr{P} v_m - h_{m,m} \mathscr{Q} v_m - h_{m-1,m} \mathscr{Q} v_{m-1} \tag{37}$$

where

$$h_{m,m} = \frac{v_m^t \mathscr{P} v_m}{v_m^t \mathscr{Q} v_m}$$
$$h_{m-1,m} = \frac{v_{m-1}^t \mathscr{P} v_m}{v_{m-1}^t \mathscr{Q} v_{m-1}}. \tag{38}$$

7) Solve the matrix equation $\mathscr{Q}\omega = f$ for ω and assign $h_{m+1,m} = \|\omega\|$.
8) Calculate the dominant eigenpair $(\lambda^{(m)}, y^{(m)})$ of the tridiagonal matrix H_m, where H_m is

$$H_m = \begin{bmatrix} h_{1,1} & h_{1,2} & & & & \\ h_{2,1} & h_{2,2} & h_{2,3} & & & \\ & h_{3,2} & h_{3,3} & & & \\ & & & \ddots & & \\ & & & & & h_{m-1,m} \\ & & & & h_{m,m-1} & h_{m,m} \end{bmatrix}. \tag{39}$$

Solving the dominant eigenpair of H_m can be done by calling EISPACK procedures. Then, check the residual norm $h_{m+1,m}|y_m^{(m)}|$ for convergence; if not converged, increment m by 1 and go to step 6.
9) Increment n_c by 1, and construct the Ritz vector. If all the desired modes have converged, then stop. Otherwise go to step 2.

D. Adaptive Mesh Refinement

In the adaptive mesh generation procedure in this paper, the degree of elements is kept fixed and only the mesh is refined. In the literature, this type of mesh refinement is called the h version.

1) A Posteriori Error Estimation: In the previous sections, the formulation was derived to solve for the electric field $\mathscr{E}$. Similarly, a variational formulation can be obtained for the magnetic field $\mathscr{H}$. To analyze the quality of the obtained solutions and obtain quantitative information about the error, we solve the problem once each for $\mathscr{E}$ and $\mathscr{H}$. As pointed out by Bossavit and Mayergoyz [10], this approach, though requiring more work, provides useful information for error analysis. This is because of the duality of $\mathscr{E}$ and $\mathscr{H}$.

Here, we provide a new procedure for computing errors in finite element solutions. This procedure is based on the reaction concept [13], [20]. By definition, the reaction of field a on source b is [13]

$$\langle a,b\rangle = \int_\Omega (\mathscr{E}^a \cdot \mathscr{J}^b - \mathscr{H}^a \cdot \mathscr{M}^b)\, d\Omega \tag{40}$$

The sources $\mathscr{J}^b$ and $\mathscr{M}^b$ can be determined from the trial fields $\mathscr{E}^b$ and $\mathscr{H}^b$ according to

$$\begin{aligned} \mathscr{J}^b &= \nabla \times \mathscr{H}^b - j\omega\epsilon\mathscr{E}^b \\ \mathscr{M}^b &= -(\nabla \times \mathscr{E}^b + j\omega\mu\mathscr{H}^b). \end{aligned} \tag{41}$$

The true field at resonance is a source-free field; thus the reaction of any field with the true source is zero. Hence, if we let $a = b$ represent a trial field and the associated source, (40) reduces to

$$\langle a,a\rangle = \int_\Omega (\mathscr{E}^a \cdot \mathscr{J}^a - \mathscr{H}^a \cdot \mathscr{M}^a)\, d\Omega = 0. \tag{42}$$

Equation (42) is the basis of the error estimation procedure presented here. By solving the problem twice, we have numerical solutions for both $\mathscr{E}$ and $\mathscr{H}$. The sources $\mathscr{J}$ and $\mathscr{M}$ are then determined from (41). Therefore, we can define an error function δ_e in each element as

$$\delta_e = \frac{\left\| \int_{\Omega_e} (\mathscr{E} \cdot \mathscr{J} - \mathscr{H} \cdot \mathscr{M})\, d\Omega \right\|}{\omega \mathscr{W}} \tag{43}$$

where

$$\mathscr{W} = \int_\Omega \left(\frac{1}{2}\epsilon \|\mathscr{E}\|^2 + \frac{1}{2}\mu \|\mathscr{H}\|^2 \right) d\Omega. \tag{44}$$

The global error δ in the numerical solutions is given by

$$\delta = \sum_e \delta_e. \tag{45}$$

2) Adaptive Procedure: Having created an initial mesh using the Delaunay triangulation [19], the next step is to refine the grid iteratively, subdividing only those elements having the largest errors. For dielectric waveguides, the procedure adopted is to solve the problem twice for $\mathscr{E}$ and $\mathscr{H}$ over the initial mesh and then to compute the error in each element separately, according to (43). The maximum element error $(\delta_e)_{\max}$ is computed. Those elements having an error greater than $0.5(\delta_e)_{\max}$ are then subdivided. This procedure is repeated until the global error is sufficiently small.

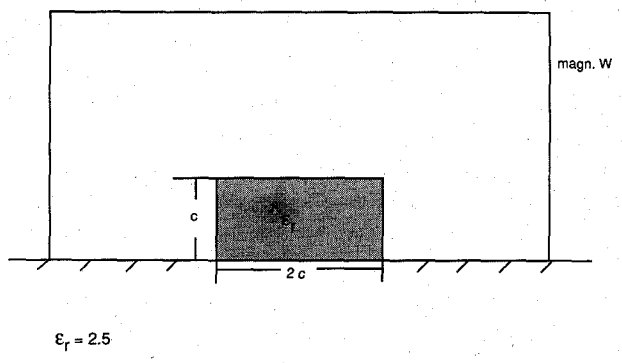

Fig. 2. Cross section of a rectangular dielectric image line.

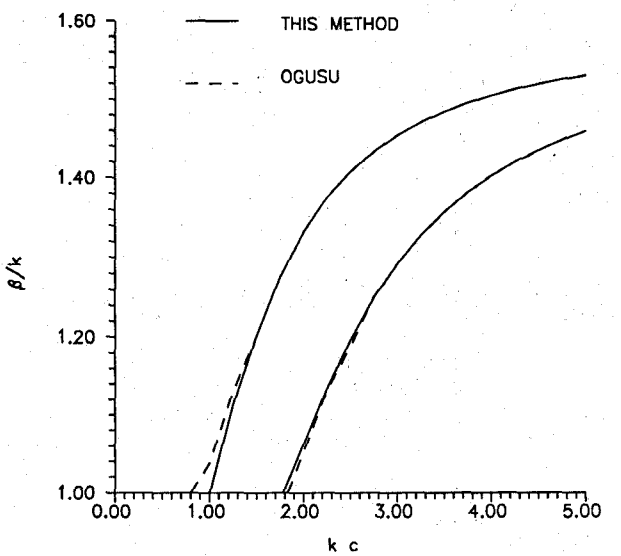

Fig. 3. Dispersion characteristics for the first two modes in the image line.

III. Numerical Results

A general-purpose computer program has been written to implement the preceding analysis. Various examples including an image guide, a microstrip transmission line, and a pedestal-supported stripline have been studied. The numerical results together with comparisons with published solutions are presented in this section.

A. An Image Guide

Fig. 2 shows the dimensions and the material properties of a rectangular dielectric image guide. Although the fields in this image guide actually extend to infinity, we have truncated the problem domain to simplify the analysis. A magnetic wall is placed on three sides of the outer boundary as indicated in Fig. 2. The computed dispersion characteristics for the first two modes are shown in Fig. 3.

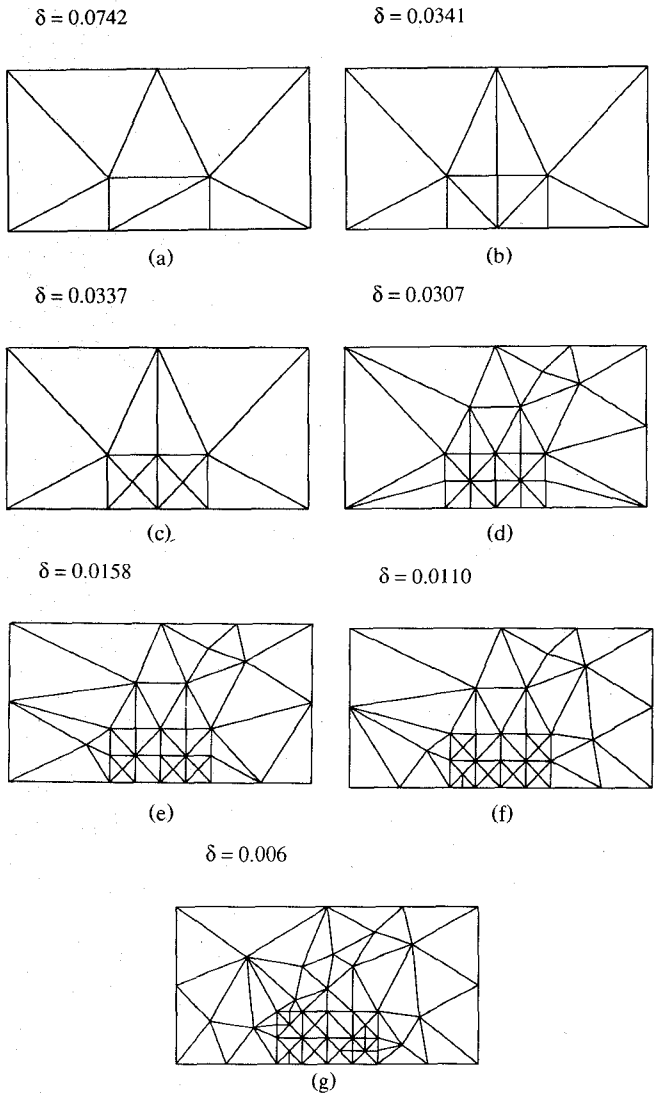

Fig. 4. Automatic mesh refinement for the image line at $kc = 2.0$.

Good agreement between these results and those of Ogusu [21] is observed.

To demonstrate the performance of the adaptive procedure, Fig. 4 show the steps in the mesh refinement for the first mode at $kc = 2$. This process is terminated when the global error δ is smaller than $1.0e-2$. The global error δ with each iteration is also indicated in the figure. As can be expected, the reaction of the field on the source is reduced by refining the mesh. The dispersion characteristics in Fig. 3 are obtained by using the final mesh in Fig. 4 throughout the entire spectrum. Fig. 5 plots the contour lines of the power distribution at $kc = 2$. It is observed from Fig. 5 that the adaptive procedure has refined the regions carrying peak power.

It is worth mentioning that the adaptive procedure results in a different mesh for each mode. This point is illustrated in Fig. 6. Fig 6(b) shows the power distribution of the second mode and is different from the power distribution of the first mode in Fig. 5. Therefore, even though both modes are computed by starting with the same initial mesh, the refined meshes in Figs. 4(g) and 6(a) for the first mode and the second mode, respectively, are not identical.

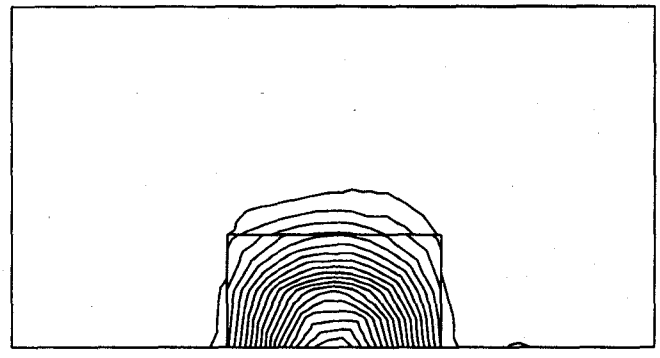

Fig. 5. Power distribution for the first mode in the image line at $kc = 2.0$.

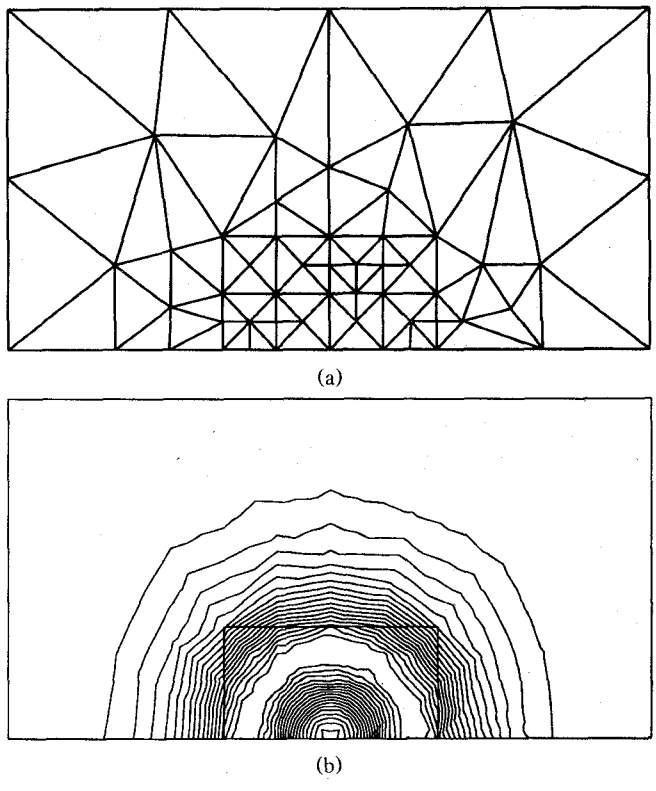

Fig. 6. The refined mesh and the power distribution for the second mode in the image line at $kc = 2.0$: (a) the refined mesh; (b) the power distribution.

B. An Infinite Thin Microstrip Line

The method presented here also applies to infinitely thin microstrip structures. However, it is necessary to take extra care in computing the $\mathscr{H}$ solution in the adaptive procedure to allow the tangential components of the $\mathscr{H}$ field to be discontinuous across the thin strip. The discon-

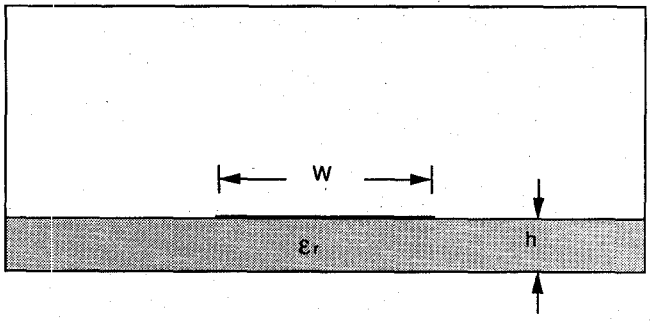

$\varepsilon_r = 11.7$

W = 12.16 mm

h = 3.04 mm

Fig. 7. A typical microstrip transmission line enclosed in a box.

$\delta = 0.0073$

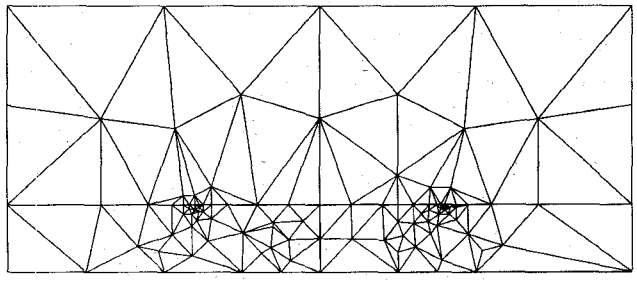

Fig. 8. The refined mesh for the microstrip generated by using the adaptive procedure at 10 GHz. $\delta = 0.0073$ in this case.

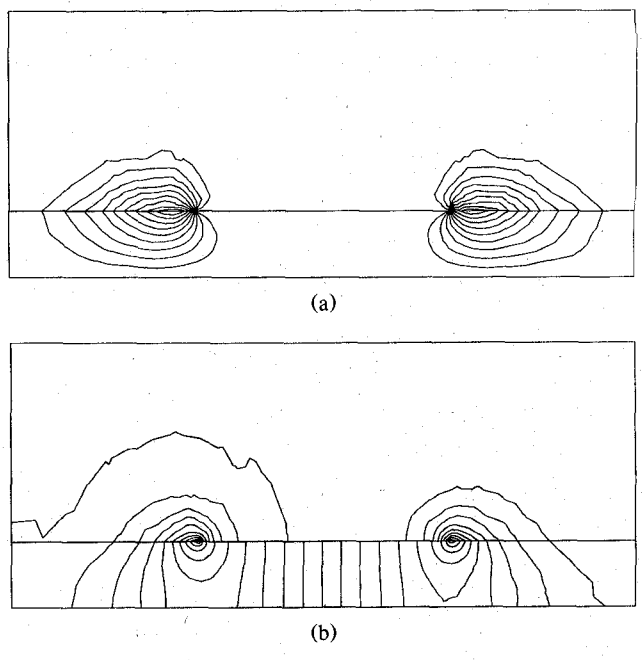

Fig. 10. Contour plots of: (a) E_z and (b) H_z for the microstrip transmission line.

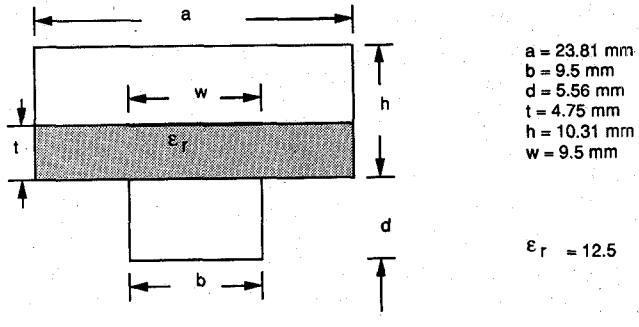

Fig. 11. Cross section of a pedestal-supported stripline.

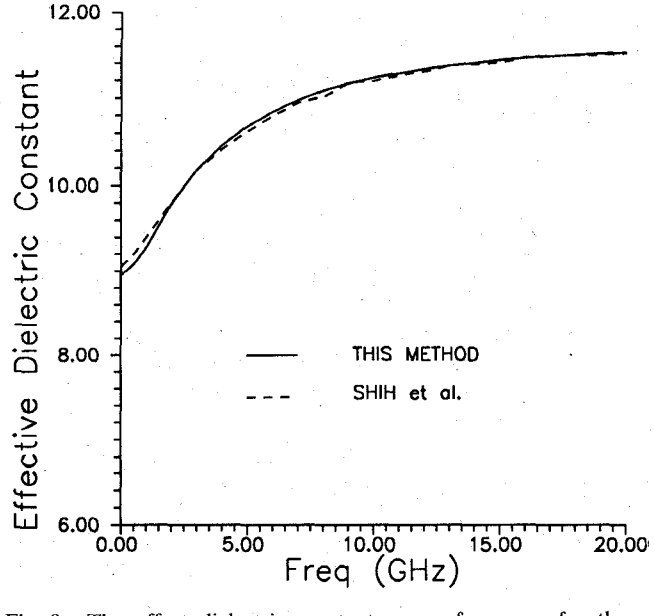

Fig. 9. The effect dielectric constant versus frequency for the microstrip transmission line.

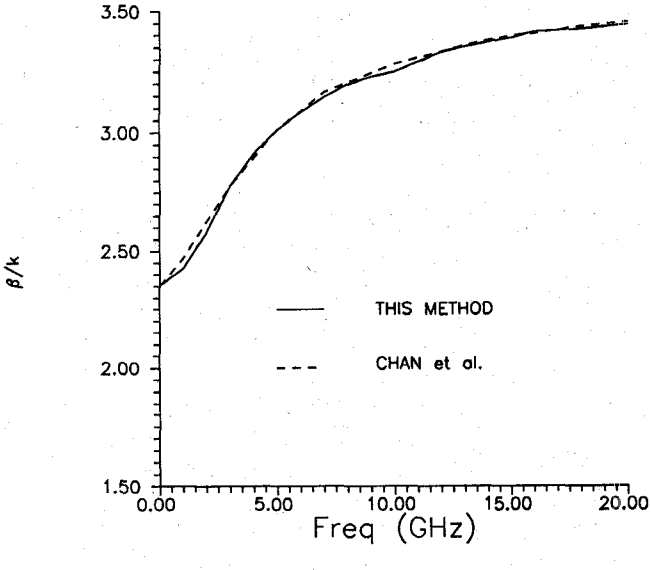

Fig. 12. Dispersion characteristics of the pedestal-supported stripline.

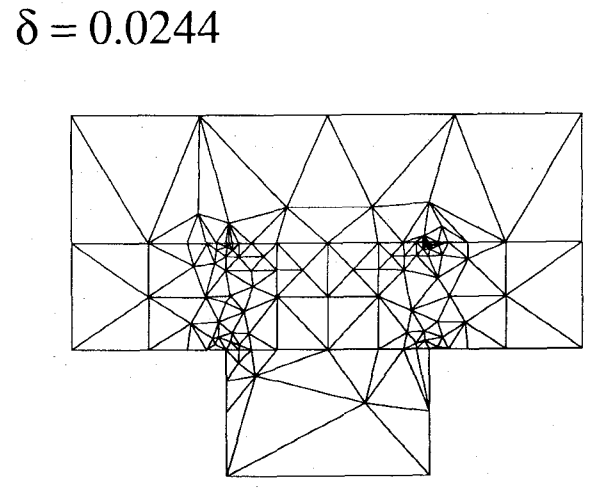

Fig. 13. The refined mesh for the pedestal-supported stripline at 10 GHz.

tinuity of the field is supported by the surface current $\mathscr{J}_s = \hat{n} \times (\mathscr{H}_1 - \mathscr{H}_2)$ that flows in the strip.

Fig. 7 shows a typical microstrip line with strip width 12.16 mm, substrate height 3.04 mm, and dielectric constant 11.7. The strip is assumed to be an infinitely thin perfect conductor. By requiring the global error δ to be smaller than 1.0e−2, the adaptive procedure generates the final mesh pattern shown in Fig. 8. It is evident from this figure that the procedure has identified the two singular points at the edges of the strip and consequently refined the grids there. The presence of the singularities degrades the accuracy of the numerical approximations and thus slows the convergence of the adaptive procedure. Therefore, it is of fundamental importance to properly model the singular points by using special elements, for example the singular elements presented in [22] and [23].

Fig. 9 presents the computed effective dielectric constant for the microstrip transmission line compared with the results in [24]. The discrepancy is at most 1.3%. Contour plots of the $\mathscr{E}_z$ and $\mathscr{H}_z$ components at 10 GHz are shown in Fig. 10. In particular, these components are high near both edges of the strip.

C. A Pedestal-Supported Stripline

A pedestal-supported stripline structure is shown in Fig. 11. The dimensions of the stripline as well as the dielectric constant are indicated in this figure. This device was investigated in [25] by using the spectral-domain approach. Our results are in agreement with those of Chan [25], as can be seen from Fig. 12. In Fig. 13, we show the refined mesh and the global error δ at 10 GHz. Since there are four singularities in this structure, the convergence of the numerical solutions is very slow. Thus, we have terminated the adaptive process with the global error $\delta = 0.0244$. Vector plots of the transverse electric field $\mathscr{E}_\tau$ and the transverse magnetic field $\mathscr{H}_\tau$ are provided in Fig. 14.

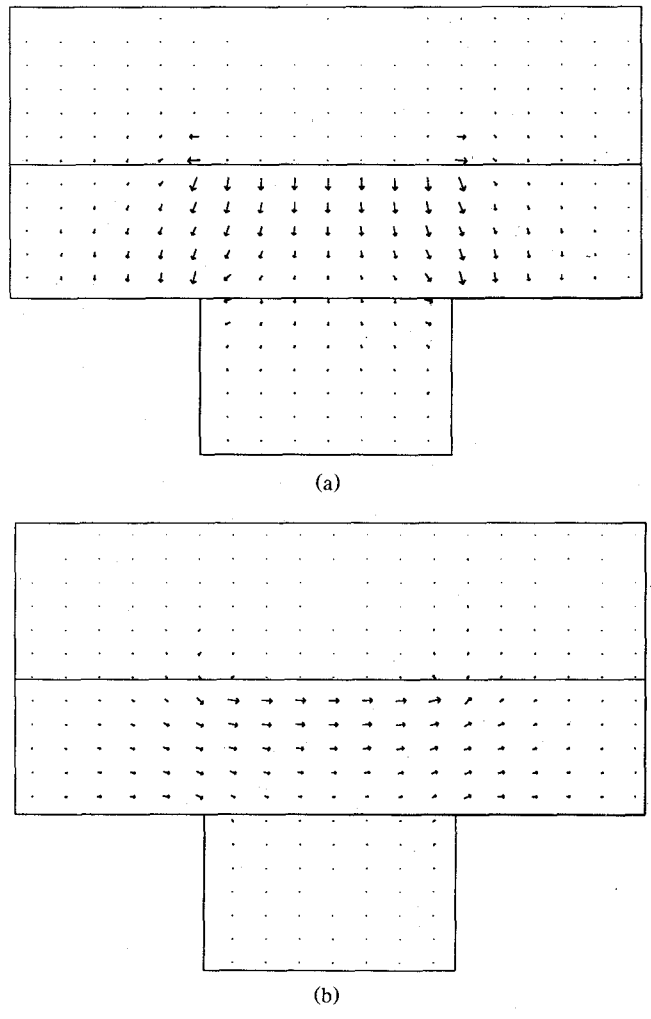

Fig. 14. Vector plots for the transverse fields in the pedestal-supported stripline at 10 GHz: (a) E_τ; (b) H_τ.

IV. Conclusion

A new numerical procedure has been presented for the full-wave analysis of dielectric waveguides. In this procedure, a novel tangential vector finite element is proposed for the electromagnetic field computation. Unlike conventional nodal finite element methods, tangential vector finite elements impose only the tangential continuity of the electric or the magnetic field across element boundaries. In this way, the new method not only matches the underlying physical requirements but also provides reliable numerical solutions. Various structures have been analyzed and numerical results compare well with those obtained elsewhere by other methods. From these structures, we have demonstrated the generality of the present analysis.

In this paper, we have also derived an error estimation procedure for the numerical solutions of dielectric waveguides. The error analysis procedure developed here is based on the reaction concept. By means of numerical examples, we have shown that this new error analysis procedure can be used to successfully automate the mesh refinement process.

ACKNOWLEDGMENT

The authors would like to thank their colleagues S. Wong, B. Shyamkumar, and A. Butler for stimulating discussions and helpful comments.

REFERENCES

[1] C. G. Williams and G. K. Cambrell, "Numerical Solution of surface waveguide modes using transverse field components," *IEEE Trans. Microwave Theory Tech.*, vol. MTT-22, pp. 329–330, Mar. 1974.
[2] T. Itoh, "Spectral domain immitance approach for dispersion characteristics of generalized printed transmission lines," *IEEE Trans. Microwave Theory Tech.*, vol. MTT-28, pp. 733–736, July 1980.
[3] E. Schwig and W. B. Bridges, "Computer analysis of dielectric waveguides: A finite-difference method," *IEEE Trans. Microwave Theory Tech.*, vol. MTT-32, pp. 531–541, May 1984.
[4] N. Schulz, K. Bierwirth, and F. Arndt, "Finite-difference analysis of integrated optical waveguides without spurious mode solutions," *Electron. Lett.*, vol. 22, no. 18, pp. 963–965, Aug. 1986.
[5] R. B. Wu and C. H. Chen, "A variational analysis of dielectric waveguides by the conformal mapping technique," *IEEE Trans. Microwave Theory Tech.*, vol. MTT-33, pp. 681–685, Aug. 1985.
[6] P. Daly, "Hybrid-mode analysis of microstrip by finite-element methods," *IEEE Trans. Microwave Theory Tech.*, vol. MTT-19, pp. 19–25, Jan. 1971.
[7] B. M. A. Rahman and J. B. Davies, "Finite-element analysis of optical and microwave waveguide problems," *IEEE Trans. Microwave Theory Tech.*, vol. MTT-32, pp. 20–28, Jan. 1984.
[8] A. J. Kobelansky and J. P. Webb, "Eliminating spurious modes in finite-element waveguides problems by using divergence-free fields," *Electron. Lett.*, vol. 22, pp. 569–570, 1986.
[9] S. H. Wong and Z. J. Cendes, "Combined finite element-modal solution of three-dimensional eddy current problems," *IEEE Trans. Magn.*, vol. 24, pp. 2685–2687, Nov. 1988.
[10] A. Bossavit and I. Mayergoyz, "Edge-elements for scattering problems," *IEEE Trans. Magn.*, vol. 25, pp. 2816–2821, July 1989.
[11] J. F. Lee, "Finite element methods for modeling passive microwave devices," Ph.D. dissertation, ECE Department, Carnegie Mellon University, June 1989.
[12] Z. J. Cendes, D. Hudak, J. F. Lee, and D. K. Sun, "Development of new methods for predicting the bistatic electromagnetic scattering from absorbing shapes," RADC-TR R&D final report, Carnegie Mellon University.
[13] R. F. Harrington, *Time Harmonic Electromagnetic Fields*. New York: McGraw-Hill, 1961.
[14] T. Angkaew, M. Matsuhara, and N. Kumagai, "Finite-element analysis of waveguide modes: A novel approach that eliminates spurious modes," *IEEE Trans. Microwave Theory Tech.*, vol. MTT-35, pp. 117–123, Feb. 1987.
[15] P. P. Silvester and R. L. Ferrari, *Finite Elements for Electrical Engineers*. Cambridge, U.K.: Cambridge University Press, 1983.
[16] B. N. Parlett, *The Symmetric Eigenvalue Problem*. Englewood Cliffs, NJ: Prentice-Hall, 1980.
[17] G. H. Golub and C. F. V. Loan, *Matrix Computations*. Baltimore, MD: Johns Hopkins University Press, 1983.
[18] B. T. Smith *et al.*, "Matrix eigensystem routines—EISPACK guide," New York: Springer-Verlag, 1976.
[19] Z. J. Cendes, D. N. Shenton, and H. Shahnasser, "Magnetic field computation using Delaunay triangulation and complementary finite element methods," *IEEE Trans. Magn.*, vol. MAG-19, pp. 2551–2554, 1983.
[20] R. B. Wu and C. H. Chen, "On the variational reaction theory for dielectric waveguides," *IEEE Trans. Microwave Theory Tech.*, vol. MTT-33, pp. 477–483, June 1985.
[21] K. Ogusu, "Numerical analysis of the rectangular dielectric waveguide and its modifications," *IEEE Trans. Microwave Theory Tech.*, vol. MTT-25, pp. 874–885, Nov. 1977.
[22] J. P. Webb, "Finite element analysis of dispersion in waveguides with sharp metal edges," *IEEE Trans. Microwave Theory Tech.*, vol. 36, pp. 1819–1824, Dec. 1988.
[23] Z. J. Cendes and J. F. Lee, "The transfinite element method for modeling MMIC devices," *IEEE Trans. Microwave Theory Tech.*, vol. 36, pp. 1639–1649, Dec. 1988.
[24] C. Shih, R. B. Wu, S. K. Jeng, and C. H. Chen, "A full-wave analysis of microstrip lines by variational conformal mapping techniques," *IEEE Trans. Microwave Theory Tech.*, vol. 36, pp. 576–581, Mar. 1988.
[25] C. H. Chan, K. T. Ng, and A. B. Kouki, "A mixed spectral-domain approach for dispersion analysis of suspended planar transmission lines with pedestals," *IEEE Trans. Microwave Theory Tech.*, vol. 37, pp. 1716–1723, Nov. 1989.

Jin-Fa Lee (S'85–M'88) was born in Taipei, Taiwan, in 1960. He received the B.S. degree from the National Taiwan University, Taiwan, in 1982 and the M.S. and Ph.D. degrees from Carnegie Mellon University, in 1986 and 1989, respectively, all in electrical engineering.

From 1988 to 1990, he was with the Ansoft Corporation, Pittsburgh, PA, where he developed several CAD/CAE finite element programs for modeling three-dimensional microwave and millimeter-wave circuits. In 1990, he left the company to pursue an academic career. Currently, he is a postdoctoral fellow at the Electromagnetic Communication Laboratory of University of the Illinois at Urbana–Champaign.

His research focuses on numerical methods for electromagnetic fields computation. Current projects include the extension of the FDTD method to nonuniform and unstructured grids, the development of local radiation boundary conditions for three-dimensional electromagnetic scattering, and the application of finite element methods for modeling optical fibers.

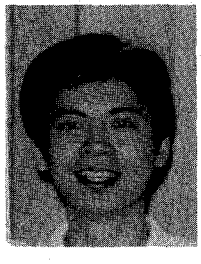

Din-Kow Sun (M'89) was born in Taipei, Taiwan, in 1956. He received the B.S. degree in physics from the National Taiwan University, Taipei, Taiwan, in 1978 and the Ph.D. degree in physics from Carnegie Mellon University, Pittsburgh, PA, in 1984.

He was a Research Associate in the Department of Electrical and Computer Engineering at Carnegie Mellon University from 1984 to 1986. Since 1986 he has been a Research Engineer at the Ansoft Corporation, Pittsburgh. His current research interests include electromagnetic theory and the development and application of numerical techniques for electromagnetics.

Zoltan J. Cendes (S'67–M'73) was born in Fefferritz, Austria, on May 16, 1946. He received the B.S. degree in science engineering from the University of Michigan in 1968 and the M.S. and Ph.D. degrees in electrical engineering from McGill University in 1970 and 1972, respectively. From 1974 to 1980, he was with the General Electric Company in Schenectady, NY, where he developed finite element tools for modeling electrostatic, electromechanical, and high-frequency electromagnetic devices. In 1980, he was appointed Associate Professor of Electrical Engineering at McGill University. He joined the Department of Electrical and Computer Engineering at Carnegie Mellon University in 1982, where he is currently Professor. He is also cofounder of the Ansoft Corporation, a supplier of electromagnetics design software. His research focuses on flexible CAE tools for electromagnetic design. Current projects include the use of Delaunay tessellation for finite element mesh generation, the development of edge-based finite elements for modeling three-dimensional electromagnetics problems, and the use of artificial intelligence to optimize engineering design parameters.

Dr. Cendes has published over 80 technical papers and was Director of the IEEE Short Course on Magnetics CAD in 1985 and 1986.